

# The one-dimensional Kardar-Parisi-Zhang and Kuramoto-Sivashinsky universality class: limit distributions

Dipankar Roy\*

Department of Mathematics, Indian Institute of Science,  
Bangalore - 560012, India.

Rahul Pandit†

Centre for Condensed Matter Theory,  
Department of Physics, Indian Institute of Science,  
Bangalore - 560012, India.

(Dated: February 1, 2022)

Tracy-Widom and Baik-Rains distributions appear as universal limit distributions for height fluctuations in the one-dimensional Kardar-Parisi-Zhang (KPZ) *stochastic* partial differential equation (PDE). We obtain the same universal distributions in the spatiotemporally chaotic, nonequilibrium, but statistically steady state (NESS) of the one-dimensional Kuramoto-Sivashinsky (KS) *deterministic* PDE, by carrying out extensive pseudospectral direct numerical simulations to obtain the spatiotemporal evolution of the KS height profile  $h(x, t)$  for different initial conditions. We establish, therefore, that the statistical properties of the 1D KS PDE in this state are in the 1D KPZ universality class.

PACS numbers: 02.30.Jr, 05.10.-a, 47.70.-n, 68.35.Rh, 74.40.Gh

Fundamental investigations of the statistical properties of hydrodynamical turbulence often use *randomly forced* versions of the *deterministic* Navier-Stokes (NS) equations (3D NSE, in three dimensions); the latter use a non-random forcing term to produce a turbulent, but nonequilibrium, statistically steady state (NESS). A randomly forced 3D, incompressible NS equation (3D RFNSE), proposed first by Edwards [1] in 1964, has been studied extensively, via renormalization-group (RG) and other theoretical [2–9] and numerical [10, 11] methods; these studies have shown that many statistical properties of turbulence in the 3D RFNSE are akin to their 3D NSE counterparts. In particular, the wave-number  $k$  dependence of the energy spectrum [12–14]  $E(k)$ , and even the mutiscaling corrections [14–18] to the Kolmogorov phenomenology [12–14] of 1941 are similar in both these models.

Can we find such similarity between the statistical properties of NESSs in *deterministic* and related *stochastic* partial differential equations (PDEs) that are simpler than their 3D hydrodynamical counterparts? It has been suggested, since the 1980s, that the Kuramoto-Sivashinsky (KS) PDE, a deterministic interface-growth model for a height field  $h(\mathbf{x}, t)$ , which is used in studies of chemical waves, flame fronts, and the surfaces of thin films flowing under gravity [19–25], is a simplified model for turbulence [23]. It has been conjectured [26], and subsequently shown by compelling numerical studies [27–32], in both one dimension (1D) and two dimensions (2D), that the long-distance and long-time behaviors of correlation functions, in the spatiotemporally chaotic NESS of the KS PDE, exhibit the same power-law scaling as their counterparts in the the Kardar-Parisi-Zhang (KPZ) equation [33–36], a stochastic PDE (SPDE), in which the height field  $h(\mathbf{x}, t)$  is kinetically roughened. The elucidation of the statistics of  $h(\mathbf{x}, t)$  in the KPZ SPDE has played a central role in nonequilibrium statis-

tical mechanics, in general, and interface-growth phenomena, in particular. Early KPZ studies [33, 34] have concentrated on height-field correlations, the width  $w(L, t)$  of the fluctuating KPZ interface, and their power-law dependences on the linear system size  $L$  and time  $t$ , for large  $L$  and  $t$  (see below); especially for the 1D case, several results can be obtained analytically. The universality of the power-law exponents has been demonstrated by explicit numerical calculations, e.g., in the poly-nuclear growth (PNG) model, directed polymers in random media (DPRM), and the asymmetric simple exclusion process (ASEP), and by experiments in turbulent liquid crystals [37–39], all of which lie (in suitable parameter regimes) in the KPZ universality class. The seminal work of Prähofer and Spohn work (recently referred to as “the 2<sup>nd</sup> KPZ Revolution” [35]) on the PNG model [40] has led to a new set of studies of the 1D KPZ universality class [36, 41–46], which have led to the remarkable result that, at a point  $x$  and at large times  $t$ ,

$$h(x, t) - h(x, 0) \approx v_\infty t + (\Gamma t)^{\beta_{\text{KPZ}}} \chi_\beta + o(t^{\beta_{\text{KPZ}}}), \text{ for } t \rightarrow \infty, \quad (1)$$

where  $v_\infty$  and  $\Gamma$  are model-dependent constants (Supplemental Material [47]), the exponent  $\beta_{\text{KPZ}} = 1/3$ , and  $\chi_\beta$  is a random variable distributed according to the Tracy-Widom (TW) distribution for the Gaussian Orthogonal Ensemble (GOE) ( $\beta = 1$ ) and for the Gaussian Unitary Ensemble (GUE) ( $\beta = 2$ ), familiar from the theory of random matrices [48], or the Baik-Rains (BR  $F_0$ ) distribution [49] ( $\beta = 0$ ); the value of  $\beta$  depends on the initial condition. We show, by extensive direct numerical simulations (DNSs), that the result (1) holds for the NESS of the 1D KS PDE. Thus, the correspondence between the statistical properties of these states, in the 1D KS (PDE) and their counterparts in the 1D KPZ (SPDE), does not stop at the simple correlation functions, investigated so far [27–30]; we demonstrate that this correspondence includes the universal

limit distributions obtained in “the 2<sup>nd</sup> KPZ Revolution” [35].

Such a result has not been obtained hitherto for a spatiotemporally chaotic NESS of a deterministic PDE.

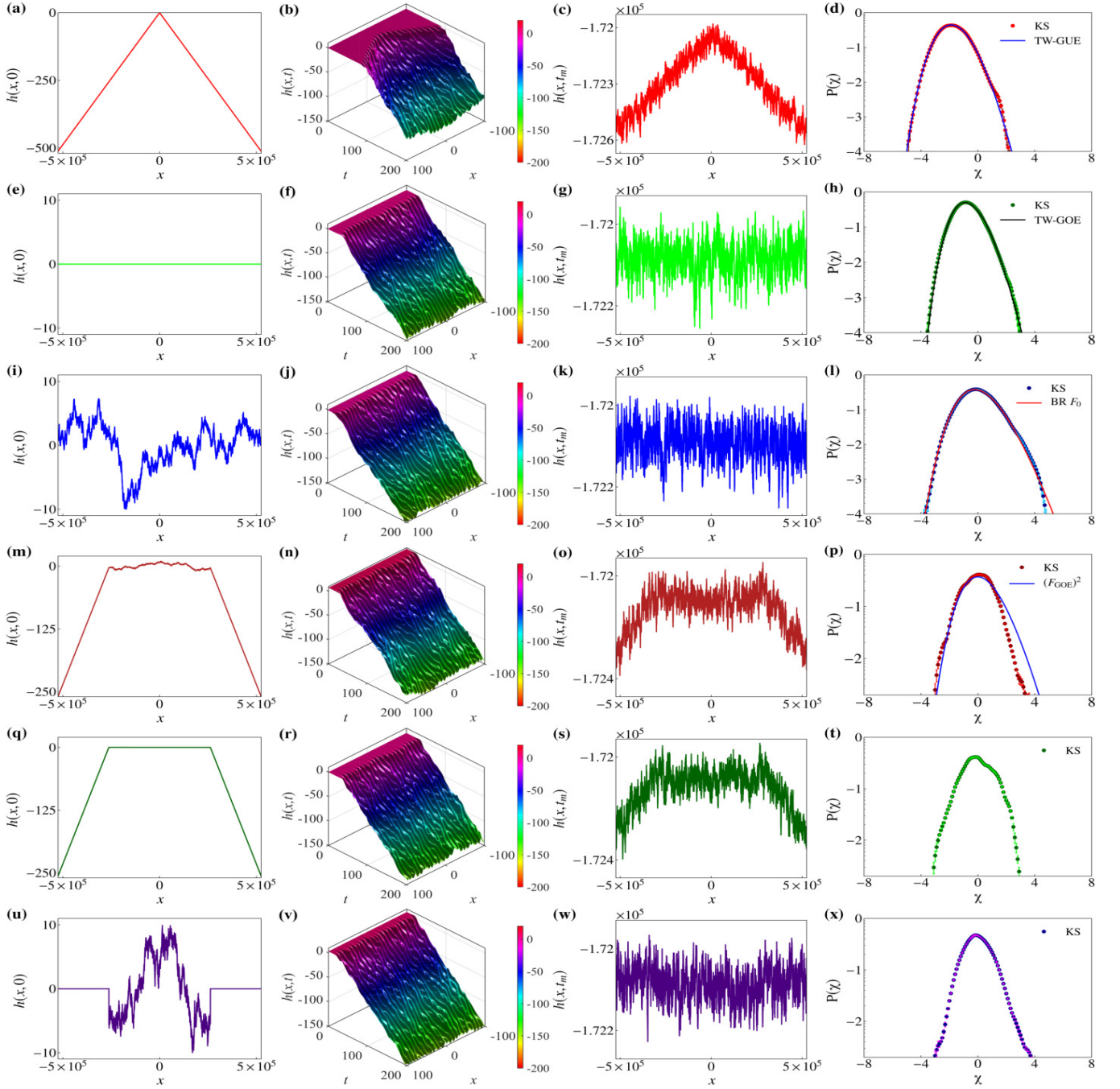


Figure 1: (Color online) Plots of  $h(x,0)$  versus  $x \in [-L/2, L/2]$ , with  $L = 2^{20}$ , for the six different initial conditions, IC1, IC2, IC3, IC4, IC5, and IC6 in (a), (e), (i), (m), (q), and (u), respectively. The short-time spatiotemporal evolution of  $h(x,t)$  is shown, in the interval  $[-100, 100]$ , for each one of IC1-IC6 in (b),(f),(j),(n),(r), and (v) (see the videos V1-V6 in the Supplemental Material [47]). The height profiles at time  $t_m = 2 \times 10^5$  are plotted in (c), (g), (k), (o), (s), and (w) for IC1-IC6, respectively; and the plots (d), (h), (l), (p), (t), and (x) display corresponding limit distributions for  $\chi$  (see text) in the NESSs; and in (d), (h), (l), and (x) we plot TW-GUE, TW-GOE, BR  $F_0$ , and  $(F_{GOE})^2$  distributions to compare them with data from our DNSs. The error bars on  $P(\chi)$  are smaller than the sizes of our symbols.

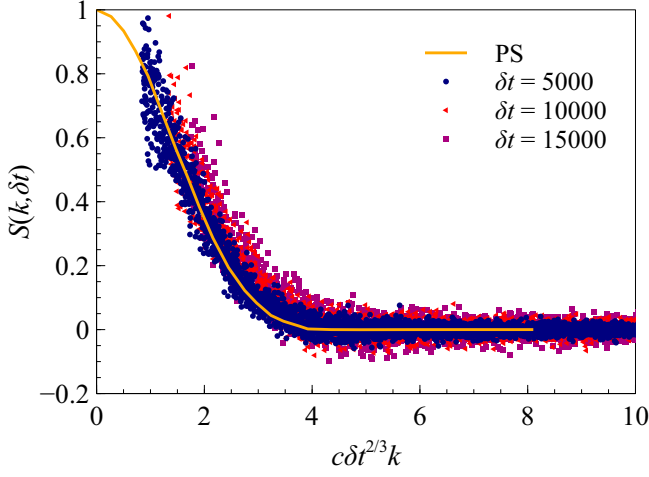


Figure 2: (Color online) Log-log plot of the scaling form of the Fourier transform of the two-point time-dependent correlation function  $S(k, \delta t)$  versus  $c\delta t^{2/3}k$ , with the nonuniversal  $c = 1.6$ , computed for IC3 (see Fig. 1(i)). We plot  $S(k, \delta t)$  for three different values of  $\delta t$ ; we also show, for comparison, the theoretical result (orange curve PS) obtained by Prähofer and Spohn [50] for the 1D KPZ equation.

The KS PDE, which predates the KPZ SPDE, is

$$\partial_t h(\mathbf{x}, t) + \Delta h(\mathbf{x}, t) + \frac{1}{2}(\nabla h(\mathbf{x}, t))^2 = 0, \quad (2)$$

where  $\nabla \equiv \partial/\partial \mathbf{x}$ ,  $\partial_t \equiv \partial/\partial t$ ,  $\Delta \equiv \nabla^2$ , and  $h$ ,  $\mathbf{x}$ , and  $t$  have been scaled such that the linear system size  $L$  is the only control parameter. The dynamical and long-wavelength properties of the 1D KS PDE have been explored via DNSs in Refs. [27–29, 51, 52]; several mathematical results have been obtained in Refs. [53–55].

The 1D KPZ SPDE is

$$\begin{aligned} \partial_t h(x, t) &= \nu \Delta h(x, t) + \frac{\lambda}{2}(\nabla h(x, t))^2 + \eta, \\ \langle \eta(x, t) \eta(x', t') \rangle &= D \delta(x - x') \delta(t - t'), \end{aligned} \quad (3)$$

where  $\nu$ , the diffusivity, and  $\lambda$ , the strength of the nonlinearity, are real parameters, and  $\eta$  is a zero-mean Gaussian white noise, with variance  $D$ .

We solve the 1D KS PDE (2), with periodic boundary conditions on a domain of size  $L$ , by using the pseudospectral method [56–58] and the 2/3 dealiasing rule. For time marching we use the fourth-order, exponential time-differencing Runge-Kutta scheme ETD RK4 [59, 60]. For reliable statistics, it is important to carry out long simulations with large values of  $L$ ; we report results with  $L = 2^{20}$ , by far the highest spatial resolution that has been used for a DNS of the 1D KS PDE (2); for this we have developed a CUDA C code that runs very efficiently on a GPU cluster with NVIDIA Tesla K80 accelerators.

From our DNSs we compute  $h(x, t)$  for six different kinds of initial conditions, IC1–IC6, which we depict by plots of  $h(x, 0)$

versus  $x$  in Figs. 1 (a), (e), (i), (m), (q), and (u); we show the short-time spatiotemporal evolution of  $h(x, t)$ , in the interval  $x \in [-100, 100]$ , in Figs. 1 (b), (f), (j), (n), (r), and (v) (see the videos V1–V6 in the Supplemental Material [47]). We choose these ICs to mimic the effect of wedge, flat, stationary, wedge-to-stationary, wedge-to-flat, and flat-to-stationary geometries in the ASEP model, which are listed in Refs. [44, 61, 62] as initial conditions for six different sub-classes of the 1D KPZ universality class. Previous numerical studies [28, 29] of the 1D KS PDE have shown that two-point, equal-time height-field correlations show the scaling behaviors of their 1D KPZ SPDE counterparts for times greater than a crossover time  $t_c \simeq 18700$  and lengths larger than the crossover size  $L_c \simeq 3600$ . Therefore, we use a very large system size  $L = 2^{20}$  and very long simulation times  $t_{max} \geq 2 \times 10^5$  (see the Supplemental Material [47]).

Our results for two-point height correlation functions are consistent with those of earlier investigations [28, 29] of the statistical properties of the spatiotemporally chaotic state of the 1D KS PDE: We show, e.g., the equal-time compensated spectrum  $k^2 E(k) = \langle L \tilde{h}(k, t) \tilde{h}^*(k, t) \rangle_t$ , where  $\langle \cdot \rangle_t$  is the time average,  $\tilde{h}(k, t)$  is the spatial Fourier transform of  $h(x, t)$ , and  $k$  is the wave number, in Fig. (1) of the Supplemental Material [47]. In addition, we calculate the time-dependent, two-point correlation function  $S(k, \delta t) = \langle k^2 \tilde{h}(k, t_0) \tilde{h}^*(k, t_0 + \delta t) \rangle_{t_0}$  in Fig. 2, for the IC3 initial condition. We find that the imaginary part of  $S(k, \delta t)$  fluctuates around zero and its magnitude is much smaller than that of its real part, which we plot in Fig. 2. Our data are consistent with the scaling form of  $S(k, \delta t)$  (orange curve in Fig. 2), which has been obtained analytically by Prähofer and Spohn [50] for the 1D KPZ SPDE; this comparison of  $S(k, \delta t)$  for the 1D KS and 1D KPZ equations has not been made hitherto.

The scaling properties of the interface width  $w(L, t)$  distinguish different universality classes in interface-growth models;

$$w(l, t) = \left( \langle [\Delta_l h(x, t)]^2 \rangle_{x,l} \right)^{1/2}, \quad (4)$$

with  $\Delta_l h(x, t) = h(x, t) - h(x, 0) - \langle h(x, t) - h(x, 0) \rangle_{x,l}$  and  $\langle \cdot \rangle_{x,l}$  the spatial average over a region of spatial extent  $l$ . For  $t \gg 1$  in the 1D KPZ equation,  $w(L, t) \sim t^\beta$ . Before crossover occurs in systems with  $L > L_c$ , the exponent  $\beta$  assumes the value  $\beta_{EW} = 1/4$ , which is the Edwards-Wilkinson (EW) result [34, 63] for the linear SPDE with  $\lambda = 0$  in Eq. (3); finally,  $\beta$  assumes the KPZ value  $\beta_{KPZ} = 1/3$  in the NESS (for  $t > t_c$ ). Moreover, the growing KPZ surface involves the length scale  $\mathcal{L}(t) \sim t^{1/z}$ , where the dynamic exponent  $z = 3/2$ ; and the width  $w(l, t) \sim l^\alpha$ , for  $l \ll \mathcal{L}(t)$ , with  $\alpha = 1/2$  [37]. We find from our DNSs of the 1D KS equation that these Family-Vicsek scaling [64] forms are indeed satisfied as we show in Figs. 3 (a), (c), and (e) for IC1–IC3 (see the Supplemental Material [47] for IC4–IC6).

We define

$$\mu_n = \langle (\Delta_L h(x, t))^n \rangle / \langle (\Delta_L h(x, t))^2 \rangle^{n/2} - 3\delta_{n,4}; \quad (5)$$

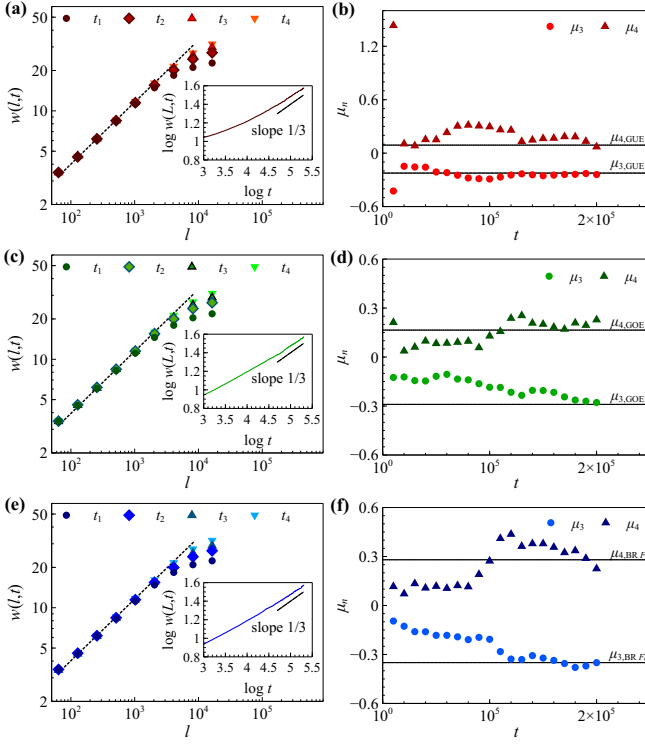


Figure 3: (Color online) Family-Vicsek scaling [64]: (a), (c), and (e) show, for IC1-IC3, respectively, plots of  $w(l, t)$  versus  $l$ , for  $l \ll L$ , and  $w(L, t)$  versus  $t$  (in the insets);  $t_1 = 5 \times 10^4$ ,  $t_2 = 10^5$ ,  $t_3 = 1.5 \times 10^5$ , and  $t_4 = 2 \times 10^5$ . The dotted lines are log-log fits for  $w(l, t) = Al^\alpha$ , with  $\alpha = 0.46 \pm 0.07$  for IC1-IC3. In (b), (d), and (f) we plot, for IC1-IC3, respectively, the skewness  $\mu_3$  and the kurtosis  $\mu_4$  (see text) versus the time  $t$ ; black lines indicate their large- $t$  values for TW-GUE, TW-GOE, and BR  $F_0$  PDFs in (b), (d), and (f). (See the Supplemental Material [47] for similar plots for IC4-IC6.)

for  $n = 3$  ( $n = 4$ ),  $\mu_n$  is the skewness (kurtosis); we plot  $\mu_3$  and  $\mu_4$  versus time  $t$  in the right panel of Fig. 3; for each initial condition, IC1-IC6, we average these quantities for 100 surfaces, over a time interval of  $10^4$ , and five independent DNS runs; i.e., our overall sample size is  $\approx 5 \times 10^8$  data points. [For our 1D KS,  $\mu_3 < 0$  because of the sign of the nonlinear term in Eq. (2); we ignore the sign of  $\mu_3$  for it can be reversed by the transformation  $h(x, t) \rightarrow -h(x, t)$ .] In addition, we calculate the probability distribution function (PDF)  $P(\chi)$  of the shifted and rescaled fluctuations, namely,  $\chi = (h(x, t) - v_\infty t)/(\Gamma t)^{1/3}$ , when both  $\mu_3$  and  $\mu_4$  are close to their standard values for the relevant TW or BR  $F_0$  PDFs; for IC2, e.g., we compute  $P(\chi)$  when we have  $\mu_3 \approx 0.27$  and  $\mu_4 \approx 0.19$ , which are close to the standard values  $\mu_{3,\text{GOE}} \approx 0.29$  and  $\mu_{4,\text{GOE}} \approx 0.16$ , respectively.

For IC1, IC2, IC3, and IC4 we compare, on semilog plots, the PDFs with TW-GUE, TW-GOE, BR  $F_0$ , and  $(F_{\text{GOE}})^2$  [44] in Figs. 1 (d), (h), (l), and (p), respectively. For ease of com-

parison, we show in Fig. 4 that the PDFs we obtain from our DNSs of the 1D KS Eq. (2) are very close to the TW-GUE, TW-GOE, and BR  $F_0$  PDFs over *at least three orders of magnitude*. Stricly speaking, we must collect data only from those two points ( $x = L/4, 3L/4$ ) at which the two different type of height profiles meet in cases IC4, IC5 and IC6. However, this leads to inadequate statistics. Therefore, the PDFs of  $\chi$  for IC4-6, which we show in Figs. 1 (t) and (x), have been computed by using data from the regions  $[7L/32, 9L/32]$  and  $[23L/32, 25L/32]$ ; we see that this averaging procedure already leads to PDFs (Figs. 1 (p), (t) and (x)) that are distinctly different from TW-GUE, TW-GOE, and BR  $F_0$  distributions.

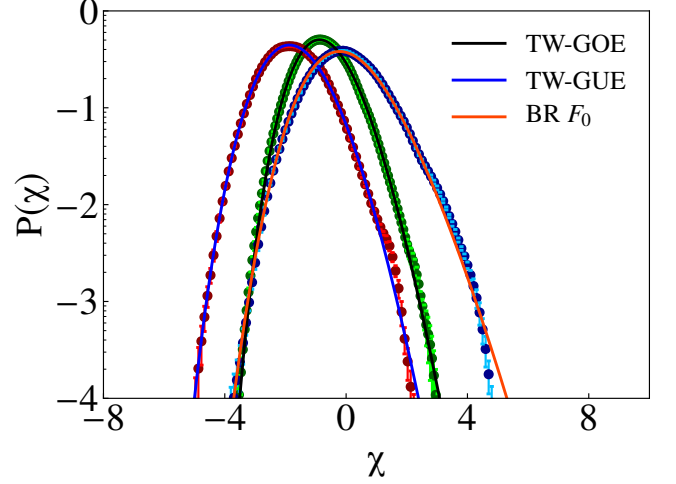


Figure 4: (Color online) Semilog plots of the PDFs  $P(\chi)$  from our DNSs for IC1, IC2, and IC3; we compare these with the Tracy-Widom distributions, TW-GUE and TW-GOE, and the Baik-Rains distributions (BR  $F_0$ ).

The TW distributions, for IC1 and IC2 initial conditions in the 1D KPZ equation, have been studied in the context of  $N \times N$  GOE ( $\beta = 1$ ) and GUE ( $\beta = 2$ ) random matrices. The largest eigenvalue (after scaling with  $N$ )  $\Lambda$  of such random matrices is

$$\Lambda = \sqrt{2} + \frac{1}{\sqrt{2}} N^{-2/3} \chi_\beta, \quad (6)$$

where  $\chi_\beta$  has the PDF [65]

$$P(\Lambda, N) \approx \begin{cases} \exp[-\beta N^2 \phi_-(\Lambda)], & \Lambda < \sqrt{2}, |\Lambda - \sqrt{2}| \sim O(1), \\ \sqrt{2} N^{2/3} P_{\text{TW},\beta}(\chi_\beta), & |\Lambda - \sqrt{2}| \sim O(N^{-2/3}), \\ \exp[-\beta N \phi_+(\Lambda)], & \Lambda > \sqrt{2}, |\Lambda - \sqrt{2}| \sim O(1), \end{cases} \quad (7)$$

$P_{\text{TW},\beta}(\chi_\beta)$  denotes TW distributions, and the right and left large-deviation functions (LDFs)  $\phi_+(\Lambda)$  and  $\phi_-(\Lambda)$ , respectively, display the following asymptotic behaviors:

$$\begin{aligned} \phi_-(\Lambda) &\approx \frac{1}{6\sqrt{2}} (\sqrt{2} - \Lambda)^3, & \Lambda \rightarrow -\infty; \\ \phi_+(\Lambda) &\approx \frac{2^{7/4}}{3} (\Lambda - \sqrt{2})^{3/2}, & \Lambda \rightarrow +\infty. \end{aligned} \quad (8)$$

The LDFs, which yield the probabilities of atypically large fluctuations, match smoothly with the tails of  $P_{TW,\beta}(\chi_\beta)$ . Because of different behaviors of the tails of  $P(\Lambda, N)$ , a third-order transition [65] can be associated with  $\Lambda$  at  $\Lambda_c = \sqrt{2}$  by defining the *free energy*  $\propto \ln F_\beta(\Lambda, N)$ ,  $F_\beta(\Lambda, N)$  being the cumulative density function (CDF) for  $\Lambda$ , for we have [65]

$$\lim_{N \rightarrow \infty} -\frac{1}{N^2} \ln F_\beta(\Lambda, N) = \begin{cases} \phi_-(\Lambda), & \Lambda < \sqrt{2}, \\ 0, & \Lambda > \sqrt{2}. \end{cases} \quad (9)$$

Similarly, we define, for the KS initial conditions IC1 and IC2, the free-energy function  $\mathcal{F}(\bar{h})$ , for  $t, L \rightarrow \infty$ , as follows:

$$\mathcal{F}(\bar{h}) = \lim_{t, L \rightarrow \infty} -\frac{1}{t^2} \ln F(\chi, t), \quad (10)$$

where  $\bar{h} = h(x, t)/t$  and  $F(\chi, t)$  is the CDF for  $\chi$  at time  $t$ . Therefore, for IC1 and IC2, we should obtain a third-order phase transition for  $\bar{h}$  at the critical value  $\bar{h}_c = v_\infty$ ; an explicit demonstration requires much better statistics for  $P(\chi)$  than is possible with our DNS.

We have shown, by extensive pseudospectral DNSs of the 1D KS deterministic PDE, that the statistical properties of its spatiotemporally chaotic NESS are in the 1D KPZ universality class. This is not limited, merely, to the power-law forms of simple correlation functions and the width of the interface. It includes, in addition, (a) the complete scaling form for the two-point time-dependent correlation function  $S(k, \delta t)$  (Fig. 2), (b) the skewness and kurtosis shown in Fig. 2, and (c) most important of all, the universal limit distributions in Fig. 1, obtained in “the 2<sup>nd</sup> KPZ Revolution” [35]. Such results have not been obtained hitherto for a spatiotemporally chaotic NESS of any deterministic PDE. We conjecture that similar conclusions should ensue for the phase-chaos regime of the 1D Complex-Ginzburg-Landau equation [25]. Such studies are also being pursued for the 1D Calogero-Moser model [66].

We thank Jaya Kumar Alageshan, R. Basu, M. Brachet, P. Ferrari, T. Imamura, K. Khanin, and K. A. Takeuchi for discussions and the National Mathematics Initiative (NMI), DST, UGC, and CSIR (India) for support.

---

\* dipankarroy@iisc.ac.in

† rahul@iisc.ac.in ; also at Jawaharlal Nehru Centre for Advanced Scientific Research, Jakkur, Bangalore 560 064

- [1] S. F. Edwards, *Journal of Fluid Mechanics* **18**, 239 (1964).
- [2] D. Forster, D. R. Nelson, and M. J. Stephen, *Phys. Rev. A* **16**, 732 (1977).
- [3] C. DeDominicis and P. C. Martin, *Phys. Rev. A* **19**, 419 (1979).
- [4] J. D. Fournier and U. Frisch, *Phys. Rev. A* **28**, 1000 (1983).
- [5] V. Yakhot and S. A. Orszag, *Journal of Scientific Computing* **1**, 3 (1986).
- [6] C.-Y. Mou and P. B. Weichman, *Phys. Rev. E* **52**, 3738 (1995).
- [7] J. K. Bhattacharjee, *Journal of Physics A: Mathematical and General* **21**, L551 (1988).

- [8] L. T. Adzhemyan, N. V. Antonov, and A. N. Vasiliev, *Physics-Uspekhi* **39**, 1193 (1996).
- [9] L. T. Adzhemyan, N. V. Antonov, and A. N. Vasiliev, *Field Theoretic Renormalization Group in Fully Developed Turbulence* (Gordon and Breach Science Publishers, 1999).
- [10] A. Sain, Manu, and R. Pandit, *Phys. Rev. Lett.* **81**, 4377 (1998).
- [11] L. Biferale, M. Cencini, A. S. Lanotte, M. Sbragaglia, and F. Toschi, *New Journal of Physics* **6**, 37 (2004).
- [12] A. N. Kolmogorov, *Dokl. Akad. Nauk SSSR* **30**, 301 (1941).
- [13] A. N. Kolmogorov, *Dokl. Akad. Nauk SSSR* **31**, 538 (1941).
- [14] U. Frisch, *Turbulence: The Legacy of A.N. Kolmogorov* (Cambridge University Press, 1995).
- [15] *Proceed. Intern. School of Physics E. Fermi, 1983, Varenna, Italy 8487*, Proceedings of the International School of Physics “Enrico Fermi”; course 88 (Amsterdam; New York : North-Holland, 1985).
- [16] R. Benzi, G. Paladin, G. Parisi, and A. Vulpiani, *Journal of Physics A: Mathematical and General* **17**, 3521 (1984).
- [17] R. Benzi and U. Frisch, *Scholarpedia* **5**, 3439 (2010).
- [18] C. Meneveau and K. R. Sreenivasan, *Journal of Fluid Mechanics* **224**, 429 (1991).
- [19] Y. Kuramoto and T. Tsuzuki, *Progress of Theoretical Physics* **55**, 356 (1976).
- [20] G. Sivashinsky, *Acta Astronautica* **4**, 1177 (1977).
- [21] G. I. Sivashinsky and D. M. Michelson, *Progress of Theoretical Physics* **63**, 2112 (1980).
- [22] C. Ruyer-Quil and P. Manneville, *The European Physical Journal B - Condensed Matter and Complex Systems* **6**, 277 (1998).
- [23] *Macroscopic Modelling of Turbulent Flows*, Lecture Notes in Physics, Vol. 230 (Springer-Verlag Berlin Heidelberg, 1985).
- [24] L.-H. Chen and H.-C. Chang, *Chemical Engineering Science* **41**, 2477 (1986).
- [25] G. Grinstein, C. Jayaprakash, and R. Pandit, *Physica D: Non-linear Phenomena* **90**, 96 (1996).
- [26] V. Yakhot, *Phys. Rev. A* **24**, 642 (1981).
- [27] J. M. Hyman, B. Nicolaenko, and S. Zaleski, *Physica D: Non-linear Phenomena* **23**, 265 (1986).
- [28] K. Sneppen, J. Krug, M. H. Jensen, C. Jayaprakash, and T. Bohr, *Phys. Rev. A* **46**, R7351 (1992).
- [29] F. Hayot, C. Jayaprakash, and C. Josserand, *Phys. Rev. E* **47**, 911 (1993).
- [30] C. Jayaprakash, F. Hayot, and R. Pandit, *Phys. Rev. Lett.* **71**, 12 (1993).
- [31] B. M. Boghosian, C. C. Chow, and T. Hwa, *Phys. Rev. Lett.* **83**, 5262 (1999).
- [32] A. Kalogirou, E. E. Keaveny, and D. T. Papageorgiou, *Proceedings of the Royal Society A: Mathematical, Physical and Engineering Sciences* **471**, 20140932 (2015).
- [33] M. Kardar, G. Parisi, and Y.-C. Zhang, *Phys. Rev. Lett.* **56**, 889 (1986).
- [34] T. Halpin-Healy and Y.-C. Zhang, *Physics Reports* **254**, 215 (1995).
- [35] T. Halpin-Healy and K. A. Takeuchi, *Journal of Statistical Physics* **160**, 794 (2015).
- [36] J. Quastel and H. Spohn, *Journal of Statistical Physics* **160**, 965 (2015).
- [37] K. A. Takeuchi, M. Sano, T. Sasamoto, and H. Spohn, *Scientific Reports* **1** (2011), 10.1038/srep00034.
- [38] K. A. Takeuchi and M. Sano, *Journal of Statistical Physics* **147**, 853 (2012).
- [39] K. A. Takeuchi, *Phys. Rev. Lett.* **110**, 210604 (2013).
- [40] M. Prähofer and H. Spohn, *Phys. Rev. Lett.* **84**, 4882 (2000).
- [41] T. Sasamoto and H. Spohn, *Phys. Rev. Lett.* **104**, 230602 (2010).
- [42] P. Calabrese and P. Le Doussal, *Phys. Rev. Lett.* **106**, 250603 (2011).

- (2011).
- [43] T. Imamura and T. Sasamoto, Phys. Rev. Lett. **108**, 190603 (2012).
  - [44] I. Corwin, Random Matrices: Theory and Applications **01**, 1130001 (2012).
  - [45] T. Halpin-Healy and Y. Lin, Phys. Rev. E **89**, 010103 (2014).
  - [46] A. A. Saberi, H. Dashti-Naserabadi, and J. Krug, Phys. Rev. Lett. **122**, 040605 (2019).
  - [47] See the Supplemental Material.
  - [48] C. A. Tracy and H. Widom, Communications in Mathematical Physics **159**, 151 (1994).
  - [49] J. Baik and E. M. Rains, Journal of Statistical Physics **100**, 523 (2000).
  - [50] M. Prähofer and H. Spohn, Journal of Statistical Physics **115**, 255 (2004).
  - [51] J. M. Hyman and B. Nicolaenko, Physica D: Nonlinear Phenomena **18**, 113 (1986).
  - [52] I. G. Kevrekidis, B. Nicolaenko, and J. C. Scovel, SIAM Journal on Applied Mathematics **50**, 760 (1990).
  - [53] P. Collet, J.-P. Eckmann, H. Epstein, and J. Stubbe, Communications in Mathematical Physics **152**, 203 (1993).
  - [54] M. Jolly, I. Kevrekidis, and E. Titi, Physica D: Nonlinear Phenomena **44**, 38 (1990).
  - [55] R. Conte and M. Musette, Journal of Physics A: Mathematical and General **22**, 169 (1989).
  - [56] C. Canuto and A. Quarteroni, CALCOLO **18**, 197 (1981).
  - [57] C. Canuto, M. Y. Hussaini, A. Quarteroni, and T. A. Zang, *Spectral Methods* (Springer-Verlag Berlin Heidelberg, 2006).
  - [58] L. N. Trefethen, *Spectral Methods in MATLAB* (SIAM, Philadelphia, 2000).
  - [59] A.-K. Kassam and L. N. Trefethen, SIAM Journal on Scientific Computing **26**, 1214 (2005).
  - [60] S. Cox and P. Matthews, Journal of Computational Physics **176**, 430 (2002).
  - [61] A. Borodin, P. L. Ferrari, and T. Sasamoto, Communications on Pure and Applied Mathematics **61**, 1603 (2008).
  - [62] I. Corwin, P. L. Ferrari, and S. Péché, Journal of Statistical Physics **140**, 232 (2010).
  - [63] S. F. Edwards and D. Wilkinson, Proceedings of the Royal Society of London. A. Mathematical and Physical Sciences **381**, 17 (1982).
  - [64] F. Family and T. Vicsek, Journal of Physics A: Mathematical and General **18**, L75 (1985).
  - [65] S. N. Majumdar and G. Schehr, Journal of Statistical Mechanics: Theory and Experiment **2014**, P01012 (2014).
  - [66] S. Agarwal, M. Kulkarni, and A. Dhar, arXiv:1903.09380.

**SUPPLEMENTAL MATERIAL: THE ONE-DIMENSIONAL  
KARDAR-PARISI-ZHANG AND KURAMOTO-SIVASHINSKY UNIVERSALITY  
CLASS: LIMIT DISTRIBUTIONS**

DIPANKAR ROY\*

*Department of Mathematics, Indian Institute of Science,  
Bangalore - 560012, India.*

RAHUL PANDIT†

*Centre for Condensed Matter Theory,  
Department of Physics, Indian Institute of Science,  
Bangalore - 560012, India.*

This Supplemental Material contains details of the calculations that we have presented in the main part of this paper.

### 1. THE COMPENSATED SPECTRUM

We show the equal-time compensated spectrum  $k^2 E(k) = \langle L \tilde{h}(k, t) \tilde{h}^*(k, t) \rangle_t$ , where  $\langle \cdot \rangle_t$  is the time average and  $\tilde{h}(k, t)$  is the spatial Fourier transform of  $h(x, t)$  and  $k$  is the wave number, in Fig. 1. The compensated spectrum  $k^2 E(k)$  that we present in Fig. 1 covers a much larger range of wave numbers than in earlier simulations [2, 5].

### 2. COMPUTATION OF THE PARAMETERS $v_\infty$ , $\Gamma$ , AND $\beta$

We compute the model-dependent parameters  $v_\infty$  and  $\Gamma$  (see Eq. (1) in the main paper) from our DNS data as follows. By choosing two Kuramoto-Sivashinsky (KS) surfaces at two different times with  $\delta t = 100$ , we compute  $\delta \langle h(x, t) \rangle_L / \delta t$ , where  $\langle \cdot \rangle_L$  is the spatial average over our simulation domain; we plot it versus time  $t$  in Fig. 2 (a); the  $t \rightarrow \infty$  limit yields  $v_\infty \simeq -0.86$ .

The exponent  $\beta$  appears in the Family-Vicsek scaling form:

$$(1) \quad w(L, t) \sim t^\beta, \text{ for } t \rightarrow \infty,$$

where  $w(L, t)$  is the width (see the main paper). To compute  $\beta$  we plot  $\log w(L, t)$  for IC2 (the flat initial condition) against  $\log t$  in Fig. 2 (b); a linear fit yields the exponent  $\beta \simeq 0.32$ , which is close to the KPZ value  $\beta_{\text{KPZ}} = 1/3$ .

In order to find the constant  $\Gamma$ , we compute  $\Sigma(t)$ , the variance of  $(h(x, t) - v_\infty t) / t^{\beta_{\text{KPZ}}}$ , and plot it versus  $t$  (see the log-log plot in Fig. 3). For  $t \gg 1$ , we have  $\Sigma(t) \rightarrow \Gamma^{2/3} \text{Var}(\chi_\beta)$ , where  $\text{Var}(\chi_\beta)$  is the variance of the random variable  $\chi_\beta$  with  $\beta = 1$  for IC2 and  $\beta = 2$  for IC1. Given that the variances of the PDFs of  $\chi_1$  and  $\chi_2$  are, respectively,  $\simeq 0.638$  and  $\simeq 0.813$  (see Ref. [4]), we compute  $\Gamma \simeq 0.358$  and  $\Gamma \simeq 0.496$  for IC1 and IC2, respectively.

---

*Date:* February 1, 2022.

\*dipankarroy@iisc.ac.in

†rahul@iisc.ac.in; also at Jawaharlal Nehru Centre for Advanced Scientific Research, Jakkur, Bangalore 560 064.

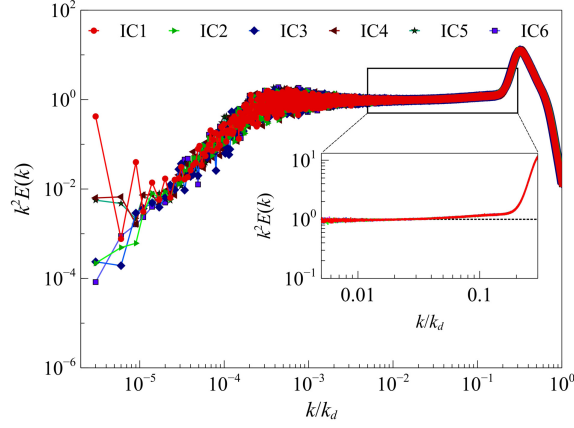


FIGURE 1. (Color online) Log-log plots of the compensated spectrum  $k^2 E(k)$  versus  $k/k_d$  for the six different initial conditions IC1-IC6 (see Fig. (1) of the main text). We zoom into the region  $\delta k/k_d = [0.005, 0.3]$ , where the curves appear flat, and show, in the inset, how our data compare with the line  $k^2 E(k) = 1$ . Here,  $k_d = \pi \lfloor L/3 \rfloor / L$  is the value of the maximum wave number after dealiasing and the system size  $L = 2^{20}$ .

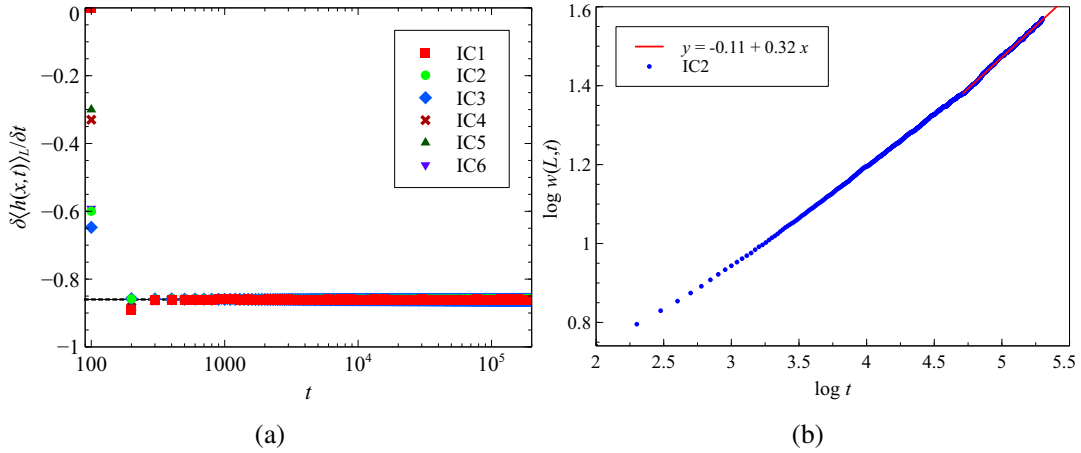


FIGURE 2. (Color online) We plot  $\langle \delta h(x, t) \rangle_L / \delta t$  versus  $t$  in (a). In (b), we display  $\log w(L, t)$  versus  $\log t$ .

### 3. FAMILY-VICSEK SCALING AND THE SKEWNESS AND KURTOSIS FOR IC4-IC6

In Figs. (4) (a)-(c) we show Family-Vicsek scaling for the initial conditions IC4-IC6. In Figs. (4) (d)-(f) we plot the skewness and kurtosis for these initial conditions. Stricly speaking, we must collect data only from those two points ( $x = L/4, 3L/4$ ) at which the two different type of height profiles meet in cases IC4, IC5, and IC6. However, this leads to inadequate statistics. Therefore, the skewness and kurtosis are computed by using data from the regions  $[7L/32, 9L/32]$  and  $[23L/32, 25L/32]$ .

### 4. SIMULATION DETAILS

We have used the exponential time-differencing fourth-order Runge-Kutta method (ETDRK4) [1, 3] for time marching in our direct numerical simulation (DNS) for the 1D KS equation. The whole simulation is programmed in CUDA C, by using the in-built *Fast Fourier Transform* in

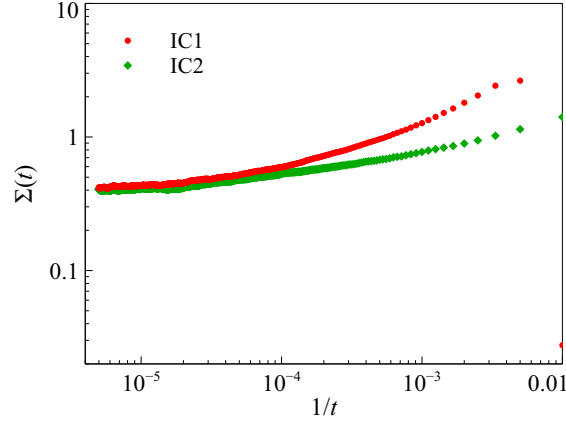
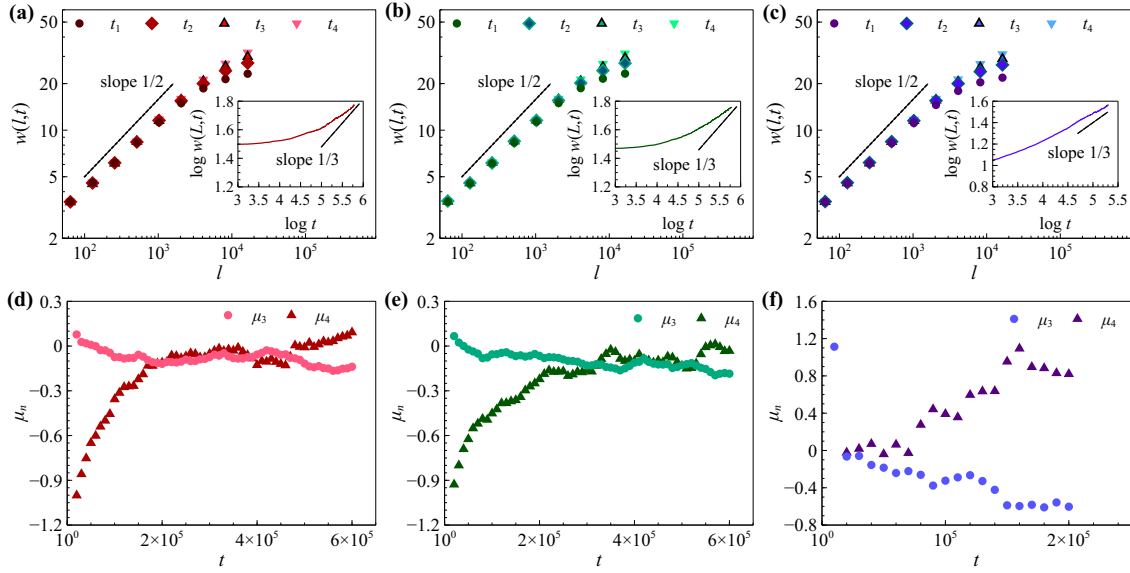

 FIGURE 3. (Color online) Log-log plots of  $\Sigma(t)$  versus  $t$  for IC1 and IC2.


FIGURE 4. (Color online) Plots of Family-Vicsek scaling in (a)-(c), and the skewness and kurtosis in (d)-(f) for IC4-IC6, respectively.

CUDA to switch back and forth between Fourier and real space in our pseudospectral DNS. Moreover, the 2/3 dealiasing rule is incorporated to avoid aliasing errors. The parameters for our DNSs are given in Table 1.

$L$	$N$	$\delta x$	$\delta t$	$t_{max}$
$2^{20}$	$2^{20}$	1	0.01	$2 - 6 \times 10^5$

TABLE 1. DNS parameters:  $L$  is the system size,  $N$  is the number of collocation points,  $\delta x = L/N$ ,  $\delta t$  is the time step, and  $t_{max}$  is the maximum time for which we run our DNS.

The evolution of  $h(x, t)$  for the six initial conditions IC1-IC6 is captured in the videos that are available at the URLs provided below:

- IC1 : <https://drive.google.com/open?id=1CPqNxda1GbntAmgHDydg3xzDRsqycxrr>
- IC2 : <https://drive.google.com/open?id=1iL154onInbzeCTzjmRJgZ-osgf6TuhcN>
- IC3 : <https://drive.google.com/open?id=1xRcXlFrETj1VqUYC5fYXeZ9s0oORw-V4>
- IC4 : <https://drive.google.com/open?id=1RULXEHa-gz4i8vGKNzH2Q54wQo4GTemw>
- IC5 : [https://drive.google.com/open?id=14rmSiAmzhBFSQ84HNj\\_9M0n7U\\_MWzzyC](https://drive.google.com/open?id=14rmSiAmzhBFSQ84HNj_9M0n7U_MWzzyC)
- IC6 : <https://drive.google.com/open?id=131uJ5mB08DCifaUovsr4i3FHN4Zh7758>

## REFERENCES

- [1] S.M. Cox and P.C. Matthews. Exponential time differencing for stiff systems. *Journal of Computational Physics*, 176(2):430 – 455, 2002.
- [2] F. Hayot, C. Jayaprakash, and Ch. Josserand. Long-wavelength properties of the kuramoto-sivashinsky equation. *Phys. Rev. E*, 47:911–915, Feb 1993.
- [3] Aly-Khan Kassam and Lloyd N. Trefethen. Fourth-order time-stepping for stiff pdes. *SIAM Journal on Scientific Computing*, 26(4):1214–1233, 2005.
- [4] Michael Prähofer and Herbert Spohn. Universal distributions for growth processes in  $1 + 1$  dimensions and random matrices. *Phys. Rev. Lett.*, 84:4882–4885, May 2000.
- [5] K. Sneppen, J. Krug, M. H. Jensen, C. Jayaprakash, and T. Bohr. Dynamic scaling and crossover analysis for the kuramoto-sivashinsky equation. *Phys. Rev. A*, 46:R7351–R7354, Dec 1992.